Fermi National Accelerator Laboratory

FERMILAB-Conf-93/166-E

E665

Ratios of Cross Sections of Carbon, Calcium and Lead at Low x_{Bj} in Inelastic Muon Scattering

Timothy J. Carroll
for the E665 Collaboration

University of Illinois at Chicago
Chicago, Illinois

Fermi National Accelerator Laboratory
P.O. Box 500, Batavia, Illinois 60510

June 1993

Presented at the *28th Rencontres de Moriond, QCD and High Energy Hadronic Interactions*, Les Arcs, Savoie, France, March 20-27, 1993

Disclaimer

RATIOS OF CROSS SECTIONS OF CARBON, CALCIUM AND LEAD AT LOW x_{Bj} IN INELASTIC MUON SCATTERING

Timothy J.Carroll
University of Illinois at Chicago
for the Fermilab E665 Collaboration
P.O. Box 500
New Muon Lab MS 356
Batavia Il. 60510 USA

Abstract

Shadowing is observed in the per nucleon cross sections of carbon, calcium and lead, as compared to deuterium. Preliminary cross section ratios are presented in the kinematic region $x_{Bj} > 0.0001$ and $Q^2 \geq 0.1$. The data were taken by Fermilab experiment E665 using inelastically scattered events from muons of mean incident momentum 468 GeV/c.

Introduction:

In the lowest order Born approximation inelastic lepton-nucleon scattering can be expressed as a double differential cross section:

$$\frac{d^2\sigma}{dx_{Bj}dQ^2} = \frac{4\pi\alpha^2 \mathrm{F}_2(x_{Bj},Q^2)}{x_{Bj}\mathrm{Q}^4}\left[1 - y_{Bj} - \frac{\mathrm{M}x_{Bj}y_{Bj}}{2\mathrm{E}} + \frac{y_{Bj}^2[1+4\mathrm{M}^2x_{Bj}^2/Q^2]}{2[1+\mathrm{R}(x_{Bj},Q^2)]}\right] \quad (1)$$

where x_{Bj} and y_{Bj} are the familiar Bjorken scaling variables, Q^2 is the negative four momentum transfer and R is the ratio of longitudinal to transverse photoabsorption cross sections. F_2 is the charge weighted quark momentum distribution. Measured per nucleon cross sections are a function of x_{Bj} as well as the atomic number of the target. As x_{Bj} approaches zero the cross section ratios of heavy nuclear targets to deuterium fall below unity. The depletion of the cross section ratio at low x_{Bj} is known as shadowing and has been observed in real as well as virtual photon scattering.[1,2,3]

Experimental Apparatus:

Fermilab experiment E665 used the world's highest energy muon beam in order to study inelastic muon scattering. Positive muons were transported to the beam spectrometer where their momentum and position were measured using 4 stations of MWPCs, two upstream and two downstream of a momentum analyzing dipole magnet. The mean beam momentum in this analysis was 468 GeV/c with an RMS of 56 GeV/c and momentum resolution, δp/p , of 0.4%.

The trajectory of each beam muon was determined using scintillating hodoscopes and was used to predict the position of the unscattered muon in a set of downstream veto hodoscopes. If no muon was detected inside an aperture defined by the beam trajectory the event was accepted as an inelastic scattering candidate. The use of this dynamic veto small angle trigger (SAT) allowed E665 to trigger at scattering angles down to 1 mr and thus to measure cross sections at Q^2 values which approach photoproduction data.

In the 1990 run of E665, targets of carbon, calcium, lead, liquid hydrogen and liquid deuterium (See Table 1) were interchanged approximately once per Tevatron cycle (58 seconds). A double dipole spectrometer, instrumented with MWPCs and drift chambers, determined the scattering angle and energy of the scattered muon upstream of 3 meters of steel which served as a hadron absorber. Additionally an electromagnetic gas sampling calorimeter was located in front of the steel. In this analysis, the calorimeter was used to identify and remove coherent muon bremsstrahlung and elastic muon-electron scatters. Muons were identified as tracks in four stations of proportional tubes and scintillating hodoscope planes located behind the steel.

Analysis:

The following cuts are applied to the data sample: $Q^2 > 0.1$ to remove non-interacting beam muons, $\nu > 50$ GeV, where ν=E-E', and $y_{Bj} > 0.1$, to remove events with poor spectrometer resolution and $y_{Bj} < 0.75$ to eliminate the kinematic region where coherent $\mu\mathrm{A} \rightarrow \mu\mathrm{A}\gamma$ scattering predominates. It is also required that the incident-scattered muon vertex be reconstructed in the target region and only one muon is reconstructed in the beam spectrometer. A phase space requirement on the incident beam is imposed which assures that the incident muon penetrated the entire target vessel. The beam requirements are also imposed on a randomly prescaled beam sample (Rbeam), which is used to correct for differences in beam flux.

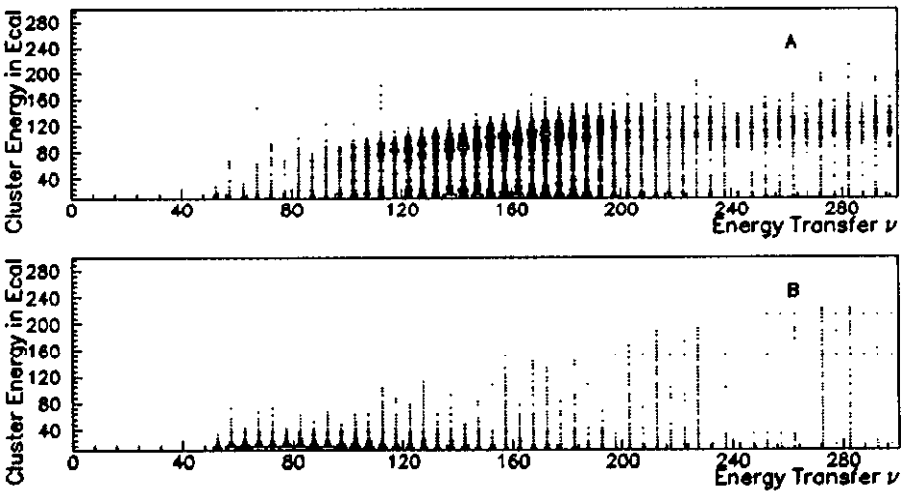

Figure 1: Cluster Energies v Energy Transfer

The distribution of cluster energies detected in the electromagnetic calorimeter is plotted against the energy transfer ν. Figure 1A) are events which have all the analysis cuts in addition to $Q^2 < 0.5\text{GeV}^2$ 1B) have $Q^2 > 2.\text{GeV}^2$.

Table 1 **Targets:** Target parameters L_I: interaction lengths, L_R: radiation lengths.

Target	Density(g/cm^2)	L_I	L_R	Triggers	Final Sample	Rbeams
Deuterium	16.2	.29	0.13	102K	15,597	81K
Carbon	30.0	.35	0.70	90K	15,118	46K
Calcium	19.5	.16	1.19	108K	14,075	70K
Lead	5.6	.03	0.89	196K	11,324	220K

These cuts eliminate spurious triggers and kinematic regions where radiative backgrounds are large. In addition, the electromagnetic calorimeter is used to identify and remove coherent muon bremsstrahlung and elastic muon-electron scatters which remain. Each cluster of energy in the calorimeter is examined and if its energy is greater than 40 GeV, the cluster is defined as an electromagnetic cluster. The energy sum of all electromagnetic clusters is normalized to the total available energy in the event, ν, and if the sum exceeds 10% the event is tagged as background and removed from the final sample. In other words,

$$\frac{\Sigma_{\text{Eclus}>40}\text{E}_{\text{Clus}}}{\nu} < 0.1. \tag{2}$$

Figure 1 shows the distribution of cluster energies versus energy transfer ν in two Q^2 regions, before calorimeter cuts. Figure 1A consists mainly of coherent bremsstrahlung scatters, which deposit a large percentage of the available energy in a single cluster, in figure 1B, the muon bremsstrahlung background is small and the cluster energies fall below 40 GeV.

The effect of cutting electromagnetic background events using the calorimeter can best be seen in the distribution of total calorimeter energy/ν versus planarity where

$$\text{Planarity} \equiv \frac{(P_\mu \times P_{\mu'}) \cdot P_\gamma}{|P_\mu||P_{\mu'}||P_\gamma|} \tag{3}$$

is a measure of the energy flow out of the muon scattering plane. Here $P_{\mu,\mu'}$ are the 3-momenta of the incident and scattered muons and P_γ is the 3-momentum of a hypothetical

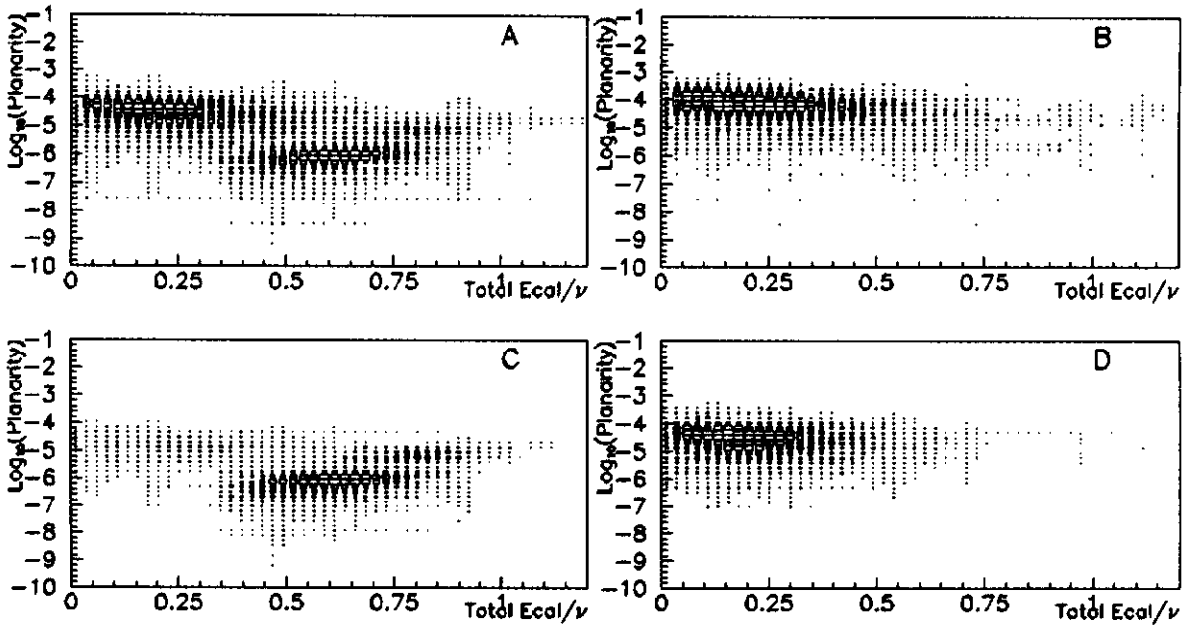

Figure 2: Ecal/ν for Identified Subsamples
The ratio Ecal/ν is a measure of the amount of final state energy which is deposited in the electromagnetic calorimeter. Plotted versus planarity for all targets, A) all events, B) events with $Q^2 > 2.\text{GeV}^2$, C) events with $Q^2 < 0.5\text{GeV}^2$ and $\nu > 100\text{GeV}$ and D) events which appear in the following cross section ratios.

bremsstrahlung photon constructed from the scattering vertex and the position of the most energetic calorimeter cluster. Figure 2 shows planarity versus total calorimeter energy/ν for all events(2A), deep inelastic scattering events(2B), background events(2C) and the events which satisfy the full set of inelastic scattering requirements(2D). In this figure the samples A, B and C where defined using tight kinematic cuts, and no calorimeter requirements. Clearly, the events which pass the final cuts are consistent with being deep inelastic scattering.

In order to check the effectiveness of using the calorimeter in this manner, a complimentary set of cuts, which rely on the fact that deep inelastic scattering events result in a high multiplicity final state, were applied. This method requires that more than two additional positive or more than two negative tracks were fitted to the muon-muon vertex in order for the event to be tagged as an inelastic scatter. This cut assumes that high multiplicity events are DIS. Results of this complimentary analysis are incomplete, but agree with the calorimeter analysis in the low x_{Bj} region where electromagnetic background removal is crucial.

Figure 3 shows the per nucleon cross section ratios for carbon, calcium and lead divided by deuterium. The x_{Bj} dependence of the systematic uncertainty is determined by varying the value of the y_{Bj} cuts and the 40 GeV calorimeter energy threshold cut. The data are adjusted for differences in beam flux by measuring the number of randomly prescaled beam events (Rbeam) which were written to tape for each target (see Table 1). Additionally, an overall systematic uncertainty due to beam flux is estimated by comparing the number of random beam triggers, per target, to the number of muon scatters that occurred in downstream detector components. The estimated uncertainty in normalization ranges from 6.3% in the carbon ratio to 1.5% in lead. The data are corrected bin by bin in x_{Bj} for empty target interactions.

The data indicate that shadowing is present in all three nuclei and the effect of shadowing

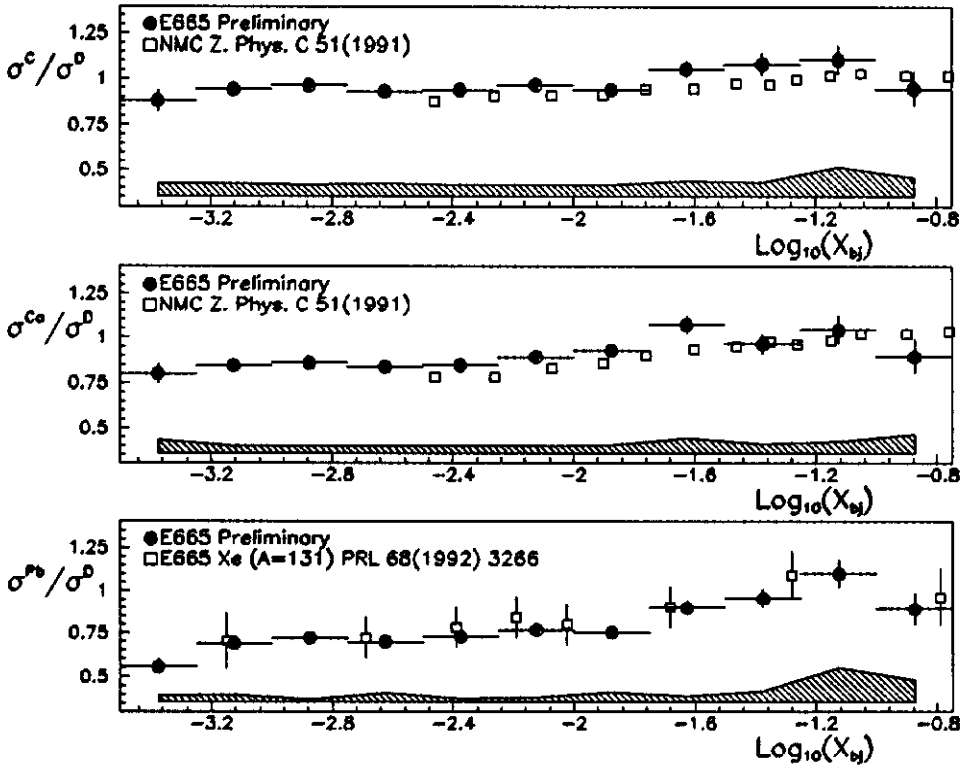

Figure 3: Cross Section Ratios v $\mathrm{Log}_{10}(x_{Bj})$

Per Nucleon cross section ratios for targets of carbon, calcium and lead as compared to deuterium. Shadowing is observed in all targets. Systematic uncertainty has been estimated and appears as a hatched band. NMC and E665 xenon errors are quoted statistical and systematic errors in quadrature.

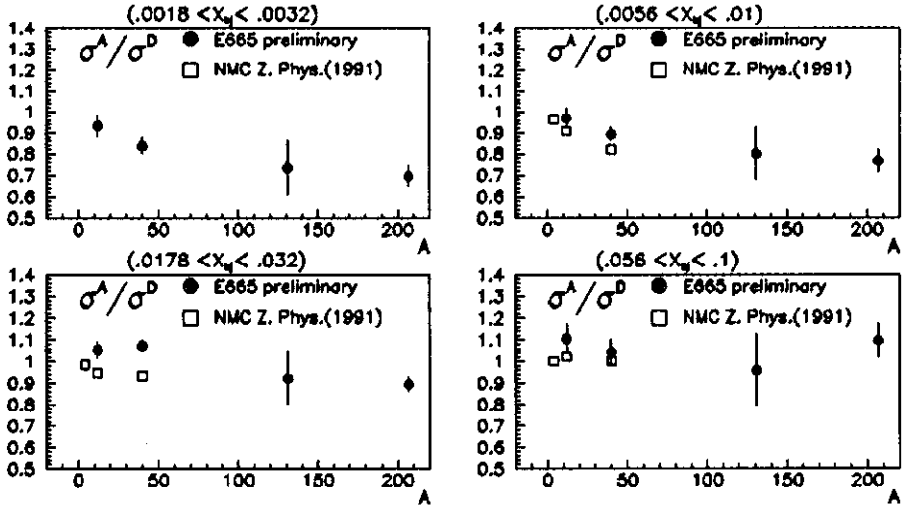

Figure 4: A dependence of Shadowing

The A dependence of Shadowing. Current results(Solid dots) are combined with data from NMC(empty box) and previously published E665 data(Solid dot A=131) to determine the A dependence of shadowing in the low, medium and high x_{Bj} regions.

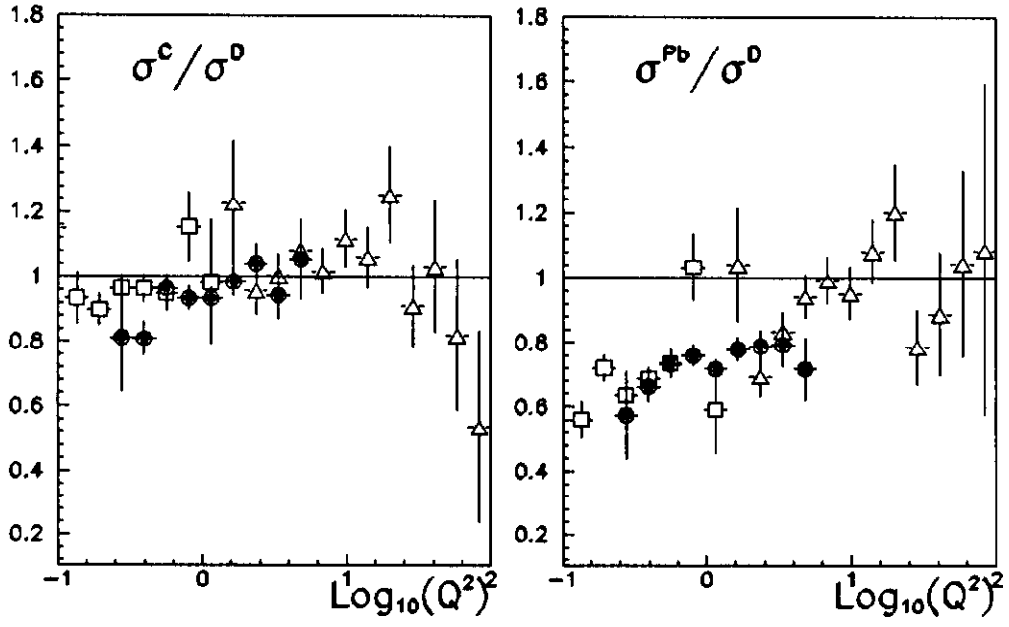

Figure 5: Q^2 Dependence of shadowing
Cross section ratios as a function of the Log of Q^2 in three x_{Bj} regions: empty box ($0.00024 < x_{Bj} < 0.0021$) full circle ($0.0029 < x_{Bj} < 0.0155$), empty triangle ($0.0160 < x_{Bj} < 0.316$).

is more pronounced in the heavier nuclear targets. The results are consistent, within errors, with previously published data.[2,3] Note that figure 3C compares cross section ratios of Xe/D to Pb/D. Figure 4 demonstrates the A- dependence of the shadowing effect, 4 x_{Bj} bins were chosen, and the cross section ratios for these bins are plotted versus atomic number, A. The bins where chosen to be equally spaced within our x_{Bj} region as well as to overlap, where possible, with previous results. The NMC and 1987 E665 results are linearly extrapolated to the center of the 1990 E665 bins. In figures 4A and 4B, the amount of shadowing is observed to increase as the atomic number increases. Finally, cross section ratios are split into three x_{Bj} regions, which were chosen to demonstrate the Q^2 dependence of shadowing. The regions were chosen to be those in which the amount of shadowing is not x_{Bj} dependent, the region in which shadowing is "turning on", and the high x_{Bj} region where no shadowing exists. Cross section ratios are plotted as a function of the logarithm Q^2 for carbon and lead. Figure 5 shows that shadowing exists at values of Q^2 above 2 GeV^2 and the weak Q^2 dependence is consistent with logarithic behavior.

Conclusion:

Cross section ratios were measured for targets of various atomic number. The ratios exhibit shadowing and are consistent with previously published data. The amount of shadowing was shown to depend on the atomic number of the target. The A dependence appears to change as the x_{Bj} of the data moves higher. Cross section ratios show weak dependence on Q^2.

References

1) D.O. Caldwell *et al.* Phys. Rev. Lett. 42(1979) 553.
2) P. Amaudruz *et al.* Z. Phys. C 51(1991) 387.
3) M.R. Adams *et al.*, Phys. Rev. Lett. 68(1992) 3266.